Macromolecular Materials and Engineering
www.mme-journal.de

Mechanical Assembly of Thermo-Responsive Polymer-Based Untethered Shape-Morphing Structures

Wei Wang

Shape-morphing robotic structures can provide innovative approaches for various applications ranging from soft robotics to flexible electronics. However, the programmed deformation of direct-3D printed polymer-based structures cannot be separated from their subsequent conventional shape-programming process. This work aims to simplify the fabrication process and demonstrates a rapid and adaptable approach for building stimulus-responsive polymer-based shape-morphing structures of any shape. This is accomplished through mechanically assembling a set of identical self-bending units in different patterns to form morphing structures using auxiliary hard connectors. A self-bending unit fabricated by a 3D printing method can be actuated upon heating without the need for tethered power sources and is able to transform from a flat shape to a bending shape. This enables the assembled morphing-structure to achieve the programmed integral shape without the need for a shape-programming process. Differently assembled morphing structures used as independent robotic mechanisms are sequentially demonstrated with applications in biomimetic morphing structures, grasping mechanisms, and responsive electrical devices. This proposed approach based on a mechanical assembling method paves the way for rapid and simple prototyping of stimulus-responsive polymer-based shape-morphing structures with arbitrary architectures for a variety of applications in deployable structures, bionic mechanisms, robotics, and flexible electronics.

1. Introduction

Shape-morphing of robotic structures with programmed shapes and volumes has highlighted a range of applications by the optimization of overall functionality via geometric changes. Shape-morphing phenomena are ubiquitous in nature and are often derived from the spatial arrangement of structural elements and their responses to external stimuli such as blooming of flowers or the hygro-morph of pine cones.[1] Shape-morphing mechanisms drawn from natural contexts based on different actuation techniques have been developed for a variety of engineering applications ranging from soft robotics to biomedical technologies.[2–6] Shape-morphing structures actuated by a tethered power source have been described based on different actuation principles such as soft pneumatic actuators,[7,8] electroactive polymers,[9,10] electrostatic actuators,[11] electromagnetic actuators,[12] and shape memory alloy-based soft actuators.[4] However, the tethered power source remains one of the major obstacles preventing these shape-morphing structures from being designed as compact and independent robotic mechanisms. Untethered shape-morphing structures with the integrated hard components of an onboard power system have been designed at the cost of sacrificing their compliance and adaptability.[13,14] Untethered small-scale shape-morphing structures with a complex internal architecture have also been developed to generate deformation but with the requirement of a cumbersome external magnetic field.[15,16] The requirement of a physical tether has resulted in a limited range of actuation and motion, whereas untethered ones have sacrificed either their adaptability or the simplicity of the mechanism designs and control appendages.

Untethered shape-morphing mechanisms can be achieved using hydrogels and shape memory polymers (SMPs) because they can respond to different environmental stimuli such as heat, humidity, and light.[17–21] Shape-morphing structures made of these two types of materials can be easily fabricated by using 3D printing as a single fabrication process.[22–25] These merits of the two materials allow for low-cost development of untethered shape-morphing mechanisms. The advantage of hydrogel-based 3D printed shape-morphing structures is that they require no subsequent programming processes after printing. However, the main shortcomings of these printed structures are their relatively low stiffness and response speed. This results in an unstable swelling actuated shape due to the subsequent loss of solvent under inconstant environmental conditions.[26–29] On the other hand, SMP-based shape-morphing structures fabricated via photopolymer ink-jetting and projection microstereolithography always require subsequent thermo-mechanical programming treatment involving

Prof. W. Wang
Department of Mechanical Engineering
Hanyang University
Seoul 04763, Republic of Korea
E-mail: davidwang@hanyang.ac.kr, hitwangw@gmail.com

The ORCID identification number(s) for the author(s) of this article can be found under https://doi.org/10.1002/mame.201900568.

DOI: 10.1002/mame.201900568

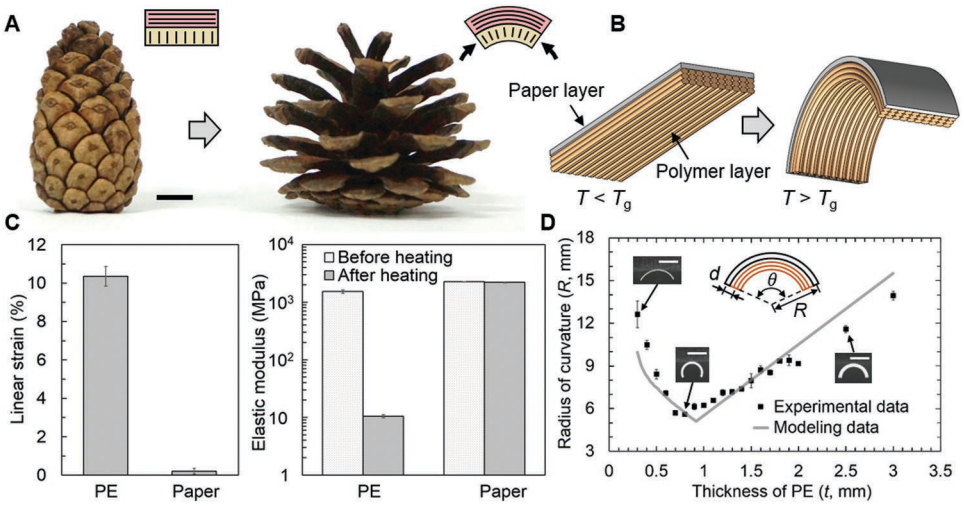

Figure 1. Working principle and performance of the self-bending units. A) A pine cone changes from its wet state to dry state. The insets indicate that the cone scale can be simplified as a bilayer with a distinct shrinking strain that forms the bending deformation. B) Bending deformation of the self-bending unit upon heating. C) Linear strain and change in the elastic modulus of the PE film and paper substrate upon heating. D) Experimental and modeling results of the bending units' minimum radius of curvature. The insets show the activated unit and its schematic with the corresponding dimensions. Scale bar: 10 mm.

multiple steps including heating, mechanical loading, cooling, and activation.[30–34] They are followed by demands for special jigs applied in mechanical loading under a well-controlled thermal environment to fix temporary shapes. In contrast, 3D printing of SMP via fused deposition modeling (FDM) is capable of simultaneously fabricating and programming without the need for any subsequent treatment processes. The deformation of these structures can be accurately accomplished by the printing parameters and the arrangement of the printed fibers layer by layer.[35–37] However, this method is valid only for fabricating shape-morphing structures with initial 2D architectures but not for 3D architectures. Therefore, versatile and convenient methods are urgently needed in order to construct SMP-based shape-morphing structures of any shape to achieve various programmable deformations.

Mechanical assembly has been a widely used approach for fabrication of both rigid and soft shape-morphing structures where a set of simple structural elements are mechanically combined as a functional mechanism. For instance, rigid structures composed of fundamental units were investigated using a kinematic synthesis approach for generating both folding and deploying motions,[38,39] and soft structures constructed through the use of elementary elastomeric units with pre-designed internal features were designed to implement multiple functions.[7,40] Hydrogel blocks were assembled with adhesion force to form 3D transformable structures.[41,42] Modular assembly has also been utilized for accelerating the construction of soft structures and robots by way of simplifying the fabrication process for intricate designs.[8,43–45] However, few research efforts have been conducted on developing stimulus-responsive polymer-based shape-morphing structures by using structure assembly.

This paper introduces a mechanical assembly approach to construct stimulus-responsive polymer-based shape-morphing structures with arbitrary architectures in a simple, fast, and economical way. The concept was applied to the construction of diverse shape-morphing assemblies with both initial 2D and 3D architectures by mechanically assembling a number of identical self-bending units in different patterns by means of auxiliary 3D printed rigid connectors. The self-bending unit in a flat strip shape was made of a polymer-paper bilayer composite fabricated by printing SMP on a paper substrate via a commercial 3D printer in a single printing process. The assembled self-bending unit is capable of transforming into a bending shape upon heating, which enables the constructed assemblies to achieve the programmed integral shapes. The approach was applied to build shape-morphing assemblies with applications to biomimetic morphing structures, robotic grippers, and responsive electrical circuits.

2. Bioinspiration and Fabrication of the Self-Bending Unit

The releasing of the seeds of a pine cone is a process of shape-morphing from a tightly packed state to an open state, which can be regarded as the combined bending deformation of each cone scale (**Figure 1**A). The cone scale shown in the insets can be considered as a bilayer structure where the cellulose microfibrils (indicated by the solid lines) in the two layers are arranged approximately perpendicular. Upon drying, the cone scale loses moisture leading to a reduction in the amount of contraction of its lower layer that is much greater than that of the upper layer. This process is due to the differently orientated cellulose microfibrils resulting in a bending deformation.[46] Inspired by the deformation of the cone scale, the basic unit used in this study is a heat-triggered self-bending bilayer structure composed of a printed polymer layer with contractile strain acting as the actuation layer. A compliant paper layer serves as the strain-limiting layer. All the bending specimens and structural components used in this work are obtained by first printing the polymer material using fused deposition

modeling (FDM) on a paper substrate to form a bilayer structure with all the printed fibers in parallel and stacked layer by layer. The obtained bilayer is then manually cut into a number of bending specimens with the required shapes for generating pure bending along the direction of the printed fibers. This allows the manufacturing of multiple actuators from a single printing process. During printing the bilayer, the molecular chains of the melted polymer fiber are stretched and aligned along the direction of extrusion, and the stretched state of the melted fiber becomes fixed and stored as memory in the printed structure. Afterward, the memorized geometry can be prompted upon heating above its glass transition temperature (T_g), resulting in a decrease in length of the printed fibers.[35] Hence, the pure bending deformation of the specimen can be achieved when the contraction of the polymer layer is resisted by the paper substrate (Figure 1B). The paper substrate used was a piece of copy paper with a thickness of 0.1 mm because of its stable mechanical properties and negligible thermal expansion coefficient. Polyester (PE) which is a type of thermo-responsive SMP with a T_g of 75 °C was chosen as the 3D printing material because of the significant heat-triggered shrinking strain of its printed fibers. The diameter of the printed fiber was determined to be 0.4 mm, which is equal to the diameter of the nozzle of the 3D printer. In addition, the amount of contraction of the printed PE layer depends on the printing parameters where the main parameters were determined as 240 °C, 40 mm s^{-1}, 0.1 mm, 110%, and 90 °C for the printing temperature, printing speed, layer thickness, filament flow, and activation temperature, respectively (Figures S1 and S2, Supporting Information). Optimizations of these parameters are not considered in this study.

Self-bending specimens and the auxiliary hard components were fabricated via FDM based 3D printers using the PE material and polycarbonate (PC) material, respectively. All the materials were commercial, and their main properties are described in the Supporting Information. The activation temperature of the self-bending specimens was determined as 90 °C, which falls in between the glass transition temperatures of PE and PC to enable the full deformation of the self-bending specimens and to ensure there are no thermal effects on the rigid components. The temperature-dependent elastic modulus and the linear strain of the paper substrate and the printed PE film were measured via a dynamic mechanical analysis (DMA) test on a DMA tester in the tension model. The testing chamber was first rapidly heated up, and then the temperature was maintained at 90 °C with a total testing time of 15 min. The linear contractile strain and change of elastic modulus of the PE film and paper substrate with respect to the increase of temperature were measured and recorded (Figure S2, Supporting Information). The results show that the final contracted strains of the printed PE film and the paper substrate were around 10.7% and 0.1%. Their corresponding reduction of the elastic modulus was around 99.3% (from 1447.5 to 10.1 MPa) and 0.5% (from 2236.5 to 2225.4 MPa), respectively (Figure 1C). As can be seen, the contracted strains and reduction of the elastic modulus of the paper substrate are negligible. The schematic of the bending specimen and its corresponding dimensions are shown in the inset of Figure 1D where the bent shape is regarded as a smooth circular arc with a bending angle of θ. The final bent shape can be obtained when a balance between the contraction of the PE layer and the paper layer is achieved. Experiments were carried out to understand the effect of different thickness of the printed PE on the maximum bending deformation of the specimen. The dimension of all the actuators was fixed at 20 × 2 mm (length × width) with the thickness of the printed PE layer printed on a 0.1 mm thick paper layer ranging from 0.3 to 3.0 mm. A mechanical model to predict the minimum bending radius of the specimens was developed based on the measured material properties (see Supporting Information). The results of the bending deformation are shown in Figure 1D. It can be seen that the mechanical model is able to predict the specimens' minimum bending radius well where there are two stages of the maximum bending deformation along with the increased PE layer's thickness. In the first stage with the PE layer's thickness smaller than around 1 mm, the achieved minimum bending radius of the specimen goes down with a thicker PE layer. This is because a thicker PE layer can produce a larger contraction force to generate a larger deformation. In the next stage with the PE layer's thickness greater than 1 mm, the outermost layer of the printed PE achieves a full contraction of 10.7%, and the bending radius gradually increases with a thicker PE layer. This variation is because the distance between the paper substrate and the PE layer was increased, resulting in a smaller bending deformation. The response speed of the bending deformation was also tested by simultaneously placing two specimens with a thickness of the PE layer of 0.5 and 1 mm, respectively, in an oven with the interior temperature maintained at 90 °C. The process of deformation of these two specimens was recorded, and results show that the deformation starting time and finishing time are around 5 and 240 s for the specimen with 0.5 mm thick PE layer, and around 15 and 600 s for the specimen with 1 mm thick PE layer.

3. Mechanical Assembly of the Morphing Structures

3.1. Proof of Concept: Mechanical Assembly

To assist in the construction of assemblies in different patterns, two different types of printed rigid connectors are used through this work including immobile joints and revolute pairs. There are predesigned slots on the connectors whose dimension is the same as that of the installation section of the bending units or structural components to achieve a stable attachment. To verify the concept of the mechanical assembly, a different number of identical units was assembled together to form shape-morphing structures with both 2D and 3D architectures (**Figure 2**) using revolute pairs. The overall dimensions of the self-bending unit are 60 × 2 × 1.1 (mm, length × width × thickness) with a fixed length of 5 mm at each end of the specimen to the rigid connectors. All of the assembled structures were activated inside an oven with a set temperature of 90 °C for 300 s. The first design consists of three identical units, which are assembled end to end using three revolute pairs to form a planar triangular shape where the specimens are installed with their PE layer facing inward to the triangle center (Figure S3,

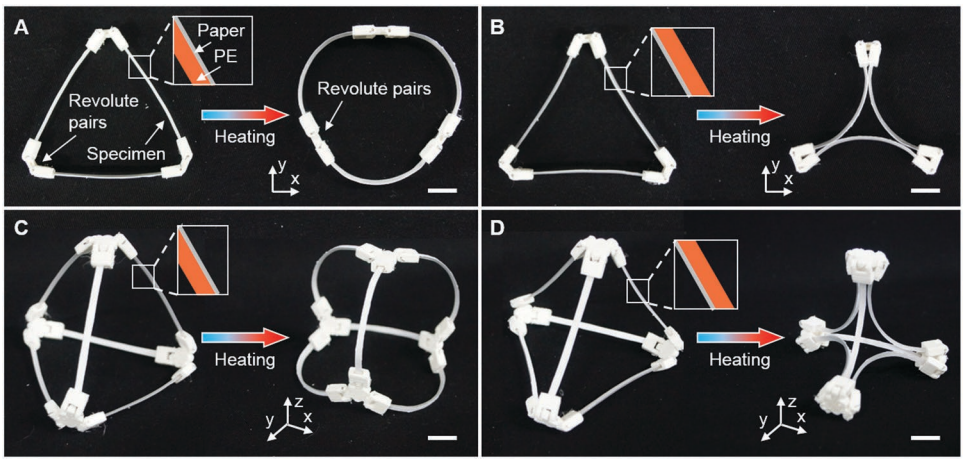

Figure 2. Shape-morphing assemblies with 2D and 3D architectures before and after activation. A,B) Triangular-shaped planar assemblies composed of three units installed with their PE layers facing inward or outward to the center show either an outward deformation or an inward deformation upon heating, respectively. C,D) Tetrahedral-shaped spatial assemblies composed of six units installed with their PE layers facing inward or outward to the center show either an outward deformation or an inward deformation upon heating, respectively. Insets show the unit schematic indicating the installation orientation of the unit. Scale bars: 10 mm.

Supporting Information). Upon heating, the specimens are bent around each central axis perpendicular to the plane to generate an expanded deformation (Figure 2A). When the specimens are assembled with their PE layer facing outward to the triangle center, an inward contractive deformation of the assembly can be achieved and vice versa (Figure 2B).

More complex assemblies with a 3D architecture can also be constructed to produce different spatial deformations based on different assembling patterns. In another demonstration, six identical units were assembled to construct an assembly in a tetrahedral shape where each vertex comprises three revolute pairs (Figure S3, Supporting Information). With all the PE layers of the assembled specimen facing inward to the centroid of the tetrahedron, the assembly can generate a spatially expanded deformation (Figure 2C). Similarly, with all the PE layers of the specimen facing outward to the centroid of the tetrahedron, an overall inward contractive deformation can be achieved (Figure 2D). It is worth mentioning that these demonstrations aim to show how the assembling pattern and the integrated deformation work in a 3D architecture rather than to optimize the performance of all the bending units. In addition, the identical units are not only limited to the suggested assembling patterns but can also be used to form a broader range of shape-morphing structures in which new designs could be introduced to perform a broader range of deformations.

3.2. Flower Mimetic Assembly

Different flower-like shape-morphing structures in previous studies have been fabricated by various direct printing approaches in which their initial configurations can only be fabricated in a 2D flat state capable of presenting a reversed process of a real flower blooming from an opened state to a closed state.[36] Otherwise, a subsequent programming process is required for these structures to show a consistent deforming process like real flower blooming.[30] To design flower-like structures with chronological blooming deformation, a set of printed PE-based 2D flat petals named as petal-1, petal-2, and petal-3 were first fabricated. All the petals were designed with an installation section at the end of the structure. The petals were then assembled to form the flower bud by inserting their installation sections to the slots of the pre-fabricated rigid receptacle (Figures S4 and S5, Supporting Information). Each petal is a bilayer that is fabricated by first printing the PE on the paper substrate and then tailoring it to the petal shapes with the same flat length of 40 mm. The printed PE layer's dimension was determined as 0.8 × 2 (mm, thickness × width) with a variable length according to different designs (**Figure 3**A, Figure S4, Supporting Information). During the assembling process, the petals were assembled with the PE layer facing outward to the center to achieve a blooming deformation. The assemblies, mentioned here and below, were activated using a heat gun with the working temperature set to 90 °C. The temperature was set much lower than the nozzle's temperature of 240 °C during the 3D printing process to prevent the petals from heat-induced damages. Heating the printed PE above its T_g, the petal transforms its configuration from a flat state to a bent state, described as the shape morphing of petal-1 in Figure 3B. In the first design, a daisy-like flower was built using 11 petal-1s forming single-layer petals. Its blooming process upon heating changed from a closed state to an opened state as illustrated in Figure 3C; Figure S5 and Movie S1, Supporting Information. Similarly, a daffodil-like flower with double-layer petals including six petal-2s and one corona was also demonstrated. The corona was fabricated by rolling the flat petal-3 into a cylinder and then installing it to the receptacle. The blooming motion of the daffodil-like flower is described in Figure 3D (Movie S2, Supporting Information). From the demonstrations, it can be seen that complex blooming structures can be constructed by mechanically assembled simple 3D printed units together.

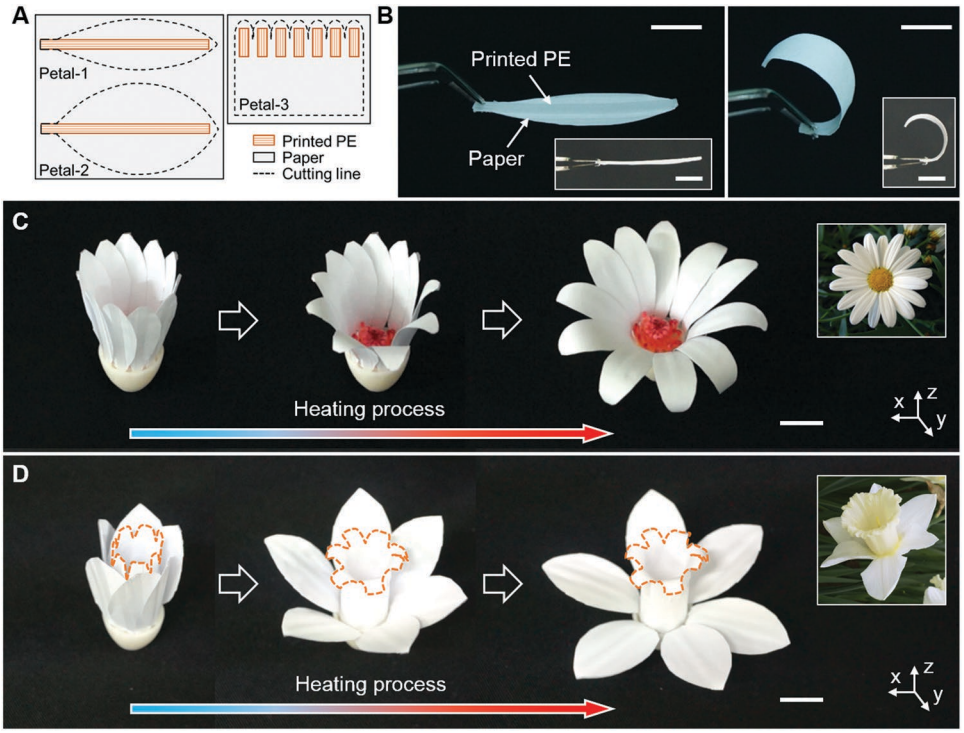

Figure 3. Assembled morphing flowers. A) Design of petal-like structures. B) Shape morphing of petal-1. Insets show the side view of the petal structure. C) Thermal-triggered chronological deformations of a daisy-like morphing flower with a single layer of petal consisting of 11 petal-1s. The inset shows the corresponding real daisy flower. D) Thermal-triggered chronological deformations of a daffodil-like morphing flower with double layers of petal consisting of six petal-2s and one corona constructed using petal-3. Dotted lines are introduced to indicate the profile of the corona. The inset shows the corresponding real daffodil flower. Scale bars: 10 mm.

3.3. Assembled Grasping Mechanisms

To demonstrate the shape-morphing structure for robotic application, multiple grasping mechanisms composed of basic identical self-bending units were designed and performed. In the first experiment, four identical bending units with dimensions of 40 × 2 × 1.1 (mm, length × width × thickness) were installed to a pre-designed rigid metacarpal with a fixed length of 5 mm for each unit so that the two opposite units were installed at an angle of 60°. The assembled gripper (gripper-1) was then used to lift a smaller cylinder-shaped object with a diameter of 15 mm (**Figure 4**A; Figure S6A and Movie S3, Supporting Information). As shown in the figure, upon heating, the gripper first generates the desired bending deformation in the low stiffness state to cage the object during the heating process, and then the deformation is maintained in a high stiffness state after the cooling process with an environmental temperature below T_g. Figure 4B (Figure S6B and Movie S4, Supporting Information) shows another customized gripper (gripper-2) composed of six identical bending units with the same dimensions in the previous design for stably grasping a slender object where the six bending units were arranged in three pairs in parallel, and each pair of units is placed oppositely at an angle of 120°.

The grasping forces generated by the grippers on the caged objects were measured by installing the activated grippers on a universal testing machine. The gripper was moved upward at a relatively slow constant speed of 150 mm min^{-1}. The grippers' vertical pulling force from caging to separating the fixed objects was measured and recorded. Gripper-1 and gripper-2 were composed of four and six bending specimens with a total self-weight of 0.72 and 2.54 g, respectively. In order to quantitatively compare the grasping performance, the grippers' force density, defined as the ratio of grasping force to the composed bending specimens' mass, of each tested gripper is plotted in Figure 4C. From the curves, both grippers' force density increases fast at the beginning and then decreases steadily along with a change in the contacting points between the gripper branch's tip and the fixed object's surface as shown in the figure insets. The results show that the maximum force density of gripper-1 and gripper-2 was around 0.37 N (0.51 N g^{-1}) and 2.22 N (0.87 N g^{-1}), that is, ≈52.4 and ≈89.2 times of their own weight (exclusive of metacarpal), respectively. It is worth noting that the force density of gripper-2 was around 1.85 times that of gripper-1. This is because the bending branches of gripper-2 have a larger bending curvature (0.05 mm^{-1}) than those of gripper-1 (0.03 mm^{-1}). This requires that the grabbed object has a larger weight to separate itself from the activated gripper by warping the gripper with a larger deformation.

By assembling identical bending units in different patterns, it is also possible to assemble grippers with an expandable deformation where the deformation can be utilized to pick up objects with specific interior characteristics. In the following

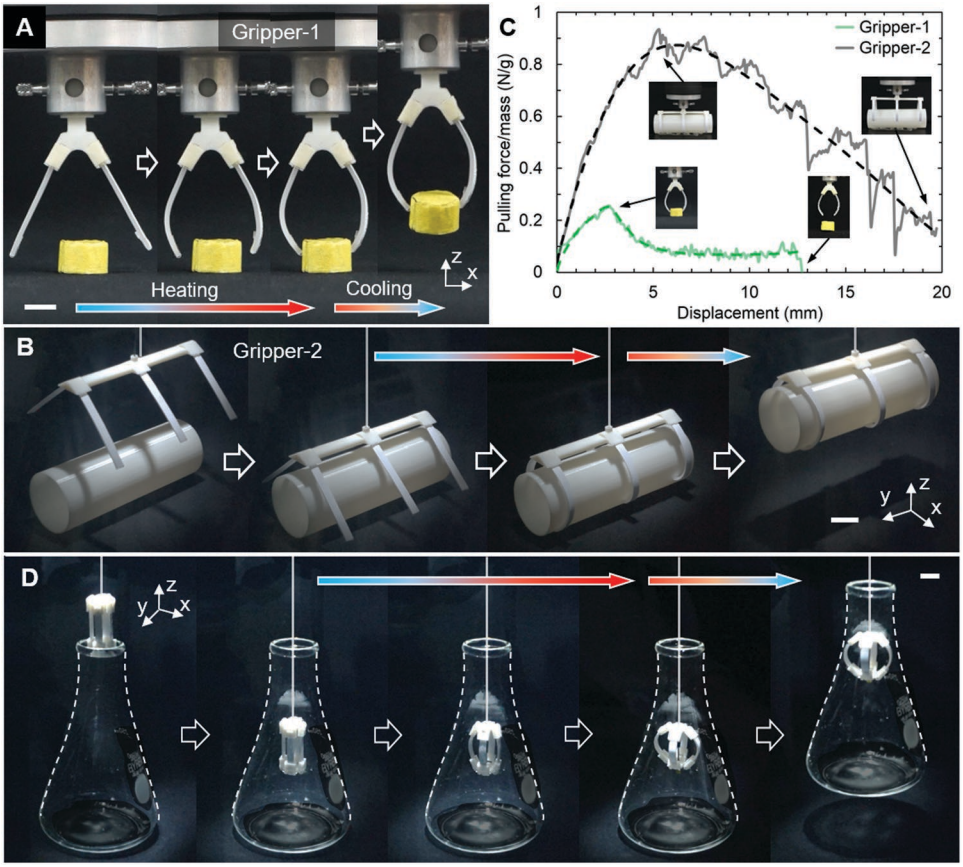

Figure 4. Assembled grasping mechanisms. A) The assembled tetrahedron-shaped gripper is used to grip a cylinder-shaped object. Dotted lines are introduced to indicate the object shape. B) The customized sideling gripper is used to grip a cylinder-shaped object with a long length. C) The grasping force of the grippers from caging to separating the fixed objects was measured as indicated in the insets. D) An assembled grasping mechanism with an expansible deformation picks up a conical glass flask by gripping the interior glass wall with a highlighted exterior wall of the flask in dashed lines. Scale bars: 10 mm.

demonstration, another grasping assembly with an expandable deformation was designed to lift a conical glass flask (weight of ≈136 g) that only has smooth glass walls without any other significant external features. One of the most effective approaches to grip such objects is to take advantage of their internal features. To do this, a gripping mechanism with an expandable deformation was designed by aligning four specimens at 90° to each other with the PE layer facing inward. The two ends of each specimen were mounted on the two pre-fabricated metacarpals by a revolving pair, respectively, with a fixed length of 5 mm (Figure S6C, Supporting Information). The gripping process is shown in **Figure 5**B (Movie S5, Supporting Information). As shown, the gripper with small and compact volume before activation was first placed inside the conical flask. After that, the gripper was activated upon heating to generate an expandable deformation wherein the diameter of the cross-section was increased to be greater than that of the bottleneck. The gripping mechanism with a retained expandable deformation after cooling can then be stuck at the bottleneck to lift the conical flask. When the deformed gripper is heated up again, the gripper can change its stiffness from the high state to the low state which can be easily taken out of the bottle using external force (Figure S7 and Movie S6, Supporting Information).

3.4. Responsive Electrical Devices

The mechanical properties of the thermo-responsive polymer-based shape-morphing assemblies were investigated. The strategies of these responsive units and their assemblies can be extended to other multi-functional structures by tailoring the characteristics of the elementary units. To explore this concept, elementary units with conductive regions were designed and utilized for constructing responsive electrical devices.[47,48] The conductive regions of the unit were formed by pasting the thin copper tape providing conductivity without significantly changing the specimen's mechanical properties. The first demonstration described an electrical temperature sensor composed of a single self-bending unit with conductive regions positioned at both ends of the specimen, which were connected using a thin and flexible conductive wire. The tailored unit is inserted in the slot of the 3D printed fixture to form an opened electrical circuit. The circuit can be connected when the unit bends, upon heated above its T_g, to contact the opposite copper tape, and then to lighten a light-emitting diode (LED) (Figure 5A; Movie S7, Supporting Information). The corresponding circuit diagrams are shown in Figure 5B. It should be noted that the tailored unit after actuation can be

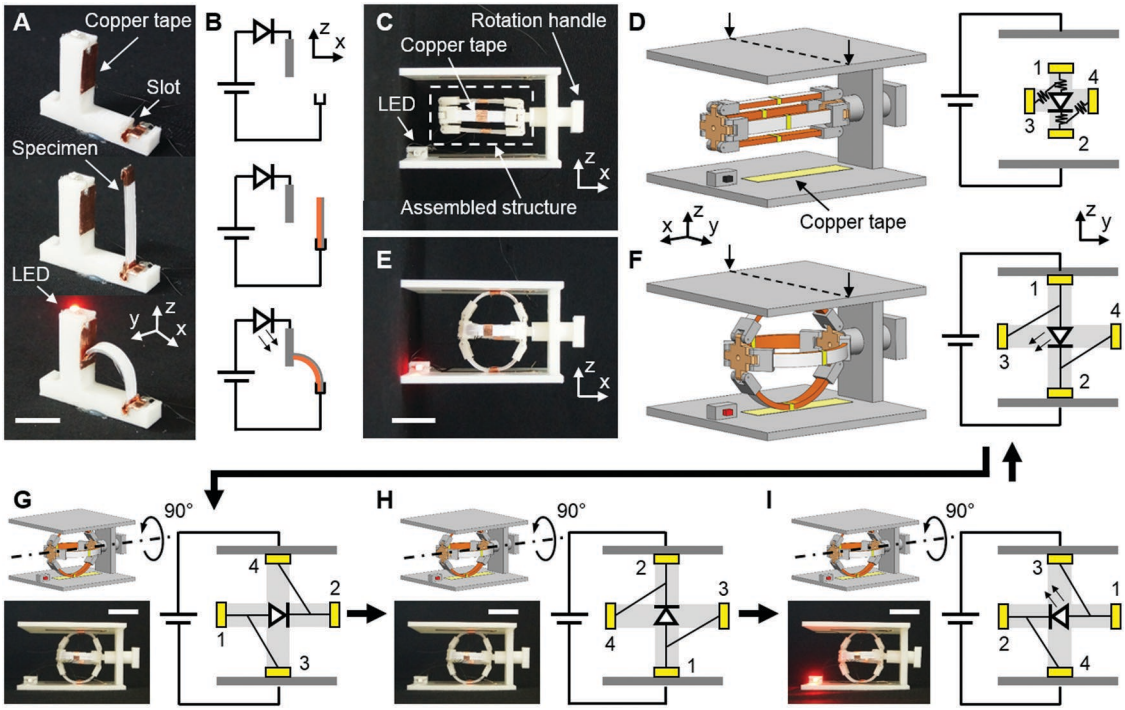

Figure 5. Responsive electrical devices. A) Fabricated fixture for the temperature sensor (top) with the tailored self-bending unit inserted in the slot to form the disconnected (middle) and connected (bottom) electrical circuit. B) Schematic showing the circuit diagram corresponding to each configuration of the temperature sensor. C,D) Photograph, schematic (parts are false-colored for visualization), and circuit diagram of the unactuated assembly placed between the positive and negative electrodes. E,F) Photograph, schematic, and circuit diagram of an expanded assembly with the lightened LED. G–I) Photographs and their corresponding schematic sequence indicating the expanded assembly with the polarity of the LED are connected in a reversed direction (G,H), a second forward direction (I), and returned to the original state (F). Scale bars: 20 mm.

conveniently replaced by inserting another unactivated unit to initiate another cycle.

The second demonstration described a circuit switch that was modified from the assembled gripping mechanism with expansible deformation (Figure 4D; Movie S8, Supporting Information). The assembly shown in Figure 5C is composed of four identical self-bending units with a conductive region positioned at the middle of each unit. The middle conductive region of each tailored self-bending unit is covered with thin copper tape. A LED is connected between the four conductive regions to form an open electrical circuit. The LED's anode and cathode were connected to two adjacent units at the conductive regions separately where the circuit diagram indicates wire connections (Figure 5D). The assembly generates a rotary motion by manually rotating the connected handle. When this assembly was placed between two conductive plates and thermally actuated, the assembly expanded, and the conductive regions on every two opposite units made electrical contact with the plates holding at a 3 V voltage difference forming a connected electrical circuit. If the polarity of the LED is correctly connected in a forward direction, the electrical current flows through the circuit to lighten the LED (Figure 5E,F). Rotating the expanded assembly disconnected the electrical contacts between the conductive regions of the specimens and the conductive plates, resulting in the LED's power-off state. In addition, inverting the direction of the expanded assembly with LED in a lightened state applies a negative bias to the LED, leading to its power-off state. Periodically manually rotating the structure enables the LED to have an intermittent illumination (Figure 5F,G; Movie S8, Supporting Information). By controlling the revolving speed of the rotation handle, the on/off state of the LED can be programmed with possible applications such as variable-frequency electronic components and information encoding.

4. Conclusions

This work describes a versatile approach to building stimulus-responsive polymer-based shape-morphing structures in 2D and 3D configurations by mechanically assembling a set of identical self-bending units in different patterns to achieve programmed integral shapes for a wide range of applications including deployable structures, bionic mechanisms, robotics, and flexible electronics. This approach of relying on a combination of fundamental units provides a novel method to fabricate stimulus-responsive polymer-based shape-morphing structures where the structures constructed by this approach are neither limited to their initial 2D configurations nor a subsequent cumbersome thermo-mechanical programming process. The proposed approach not only enables rapid and simple prototyping of various shapes of geometrical complexity but also shortens the fabrication time while simplifying the fabrication process significantly. The assembled shape-morphing structures were

demonstrated by constructing different soft morphing flowers and gripping mechanisms. Additional functionalities, as an example of electrical conductivity, can be incorporated into the final designs. This concept was initially explored by the illumination of an LED. However, it could be extended to more advanced applications ranging from variable-frequency electronic components to information encoding. The temperature to induce deformation was set as 90 °C, which is much lower than the 3D printing temperature of PE (≈240 °C) to avoid the heat-induced damages or failures of the morphing specimens and structures. All the bending units and structural components were manually tailored from a bilayer structure which was manufactured from off-the-shelf materials by means of 3D printing. This printing process can be scaled through the use of a large number of deposition nozzles with a larger substrate. The manual cutting process can easily be replaced by using laser cutting or other rapid cutting methods and patterning algorithms can also be used to optimize material use. This would allow for the rapid and adaptable parallel fabrication of stimulus-responsive structures with arbitrary architectures for future commercialization. The proposed approach in this study was accomplished by using thermo-responsive polymer-based specimens, however, this approach can be applied to construct morphing structure made of other responsive materials that can respond to different environmental stimuli such as heat, humidity, and light.

It should be noted that the self-bending unit is not only limited to the proposed shape-morphing structures but also forms a broader range of shape-morphing structures based on different assembly patterns. Additional units with different designs (e.g., size, shape, deformation) could be introduced to enable a broader range of assemblies. It is noticed that the actuation speed of the unit and assemblies in this study is slower than the reported ones in previous studies. This is because the designs in this study had a thickness of 1 mm, which is much thicker than their reported counterparts, resulting in requirements of a long time for absorbing heat energy to generate the deformations. The main reason for choosing paper as a substrate in this work is that paper is ubiquitous and lightweight. Because of the paper's stable mechanical properties and negligible thermal expansion coefficient, the specimens were designed with irreversible deformation. However, based on different phase-changing temperature or different thermal expansion coefficient, composite polymers composed of different responsive materials or the same material with anisotropic fabrication parameters could be utilized to achieve reversible deformations to be presented in future work. Besides, all the designs are described in centimeter-scale, however, by exploiting the scale-free geometric features of the morphing actuators and by virtue of advanced microscale manufacturing technologies, the proposed approach can be extended to microscale structures simplifying the way to design morphing structures with tailored properties over a wide range of dimensions.

Supporting Information

Supporting Information is available from the Wiley Online Library or from the author.

Acknowledgements

The author would like to thank S. Ye for the key inputs. This work was supported by the National Research Foundation of Korea (NRF) grant funded by the Korea government (MSIT) (No. 2019R1F1A1062619), and by the research fund of Hanyang University (HY-2019).

Conflict of Interest

The author declares no conflict of interest.

Keywords

3D printing, biomimetics, responsive electrical devices, shape memory polymers, soft robots, stimulus-responsive polymers

Received: August 27, 2019
Revised: September 25, 2019
Published online: November 10, 2019

[1] E. Reyssat, L. Mahadevan, *J. R. Soc., Interface* **2009**, *6*, 951.
[2] C. L. Randall, E. Gultepe, D. H. Gracias, *Trends Biotechnol.* **2012**, *30*, 138.
[3] S. Felton, M. Tolley, E. Demaine, D. Rus, R. Wood, *Science* **2014**, *345*, 644.
[4] W. Wang, S. Ahn, *Soft Rob.* **2017**, *4*, 1.
[5] W. Coral, C. Rossi, O. M. Curet, D. Castro, *Bioinspiration Biomimetics* **2018**, *13*, 056009.
[6] Q. Zhao, Y. Wang, H. Cui, X. Du, *J. Mater. Chem. C* **2019**, *7*, 6493.
[7] S. A. Morin, S. W. Kwok, J. Lessing, J. Ting, R. F. Shepherd, A. A. Stokes, G. M. Whitesides, *Adv. Funct. Mater.* **2014**, *24*, 5541.
[8] S. W. Kwok, S. A. Morin, B. Mosadegh, J. H. So, R. F. Shepherd, R. V. Martinez, B. Smith, F. C. Simeone, A. A. Stokes, G. M. Whitesides, *Adv. Funct. Mater.* **2014**, *24*, 2180.
[9] M. T. Christianson, C. Goldberg, N. N. Deheyn, D. D. Cai, S. Tolley, *Sci. Rob.* **2018**, *3*, eaat1893.
[10] J. Cao, W. Liang, J. Zhu, Q. Ren, *Bioinspiration Biomimetics* **2018**, *13*, 066005.
[11] E. Acome, S. K. Mitchell, T. G. Morrissey, M. B. Emmett, C. Benjamin, M. King, M. Radakovitz, C. Keplinger, *Science* **2018**, *359*, 61.
[12] T. N. Do, H. Phan, T. Q. Nguyen, Y. Visell, *Adv. Funct. Mater.* **2018**, *28*, 1800244.
[13] S.-H. Song, M.-S. Kim, H. Rodrigue, J.-Y. Lee, J.-E. Shim, M.-C. Kim, W.-S. Chu, S.-H. Ahn, *Bioinspiration Biomimetics* **2016**, *11*, 036010.
[14] T. Li, G. Li, Y. Liang, T. Cheng, J. Dai, X. Yang, B. Liu, *Sci. Adv.* **2017**, *3*, e1602045.
[15] W. Hu, G. Z. Lum, M. Mastrangeli, M. Sitti, *Nature* **2018**, *554*, 81.
[16] S. Tottori, L. Zhang, F. Qiu, K. K. Krawczyk, A. Franco-Obregõn, B. J. Nelson, *Adv. Mater.* **2012**, *24*, 811.
[17] S. Agarwal, S. Jiang, Y. Chen, *Macromol. Mater. Eng.* **2019**, *304*, 1800548.
[18] X. Du, H. Cui, Q. Zhao, J. Wang, H. Chen, Y. Wang, *Research* **2019**, *2019*, 6398296.
[19] L. Huang, R. Jiang, J. Wu, J. Song, H. Bai, B. Li, Q. Zhao, T. Xie, *Adv. Mater.* **2017**, *29*, 1605390.
[20] Y. Wang, H. Cui, Q. Zhao, X. Du, *Matter* **2019**, *1*, 626.
[21] Q. Zhao, J. Wang, H. Cui, H. Chen, Y. Wang, X. Du, *Adv. Funct. Mater.* **2018**, *28*, 1870202.
[22] Y. Zhou, W. M. Huang, S. F. Kang, X. L. Wu, H. B. Lu, J. Fu, H. Cui, *J. Mech. Sci. Technol.* **2015**, *29*, 4281.

[23] F. Momeni, S. M. M. H. N, X. Liu, J. Ni, *Mater. Des.* **2017**, *122*, 42.
[24] V. Khare, S. Sonkaria, G. Y. Lee, S. H. Ahn, W. S. Chu, *Int. J. Pr. Eng. Man.-GT* **2017**, *4*, 291.
[25] Q. Ge, C. K. Dunn, H. J. Qi, M. L. Dunn, *Smart Mater. Struct.* **2014**, *23*, 094007.
[26] A. Sydney Gladman, E. A. Matsumoto, R. G. Nuzzo, L. Mahadevan, J. A. Lewis, *Nat. Mater.* **2016**, *15*, 413.
[27] T. Chen, H. Bakhshi, L. Liu, J. Ji, S. Agarwal, *Adv. Funct. Mater.* **2018**, *28*, 1800514.
[28] J. C. Breger, C. Yoon, R. Xiao, H. R. Kwag, M. O. Wang, J. P. Fisher, T. D. Nguyen, D. H. Gracias, *ACS Appl. Mater. Interfaces* **2015**, *7*, 3398.
[29] Y. Zhang, R. An, L. Han, X. Wang, L. Shi, R. Ran, *Macromol. Mater. Eng.* **2018**, *303*, 2.
[30] Q. Ge, A. H. Sakhaei, H. Lee, C. K. Dunn, N. X. Fang, M. L. Dunn, *Sci. Rep.* **2016**, *6*, 31110.
[31] M. Zarek, M. Layani, I. Cooperstein, E. Sachyani, D. Cohn, S. Magdassi, *Adv. Mater.* **2016**, *28*, 4449.
[32] Y. Sun, M. Chu, M. Huang, O. Hegazi, H. E. Naguib, *Macromol. Mater. Eng.* **2019**, *304*, 1900196.
[33] H. Wei, Q. Zhang, Y. Yao, L. Liu, Y. Liu, J. Leng, *ACS Appl. Mater. Interfaces* **2017**, *9*, 876.
[34] F. Ji, X. Liu, C. Lin, Y. Zhou, L. Dong, S. Xu, D. Sheng, Y. Yang, *Macromol. Mater. Eng.* **2019**, *304*, 1800528.
[35] W. Wang, C. Li, M. Cho, S.-H. Ahn, *ACS Appl. Mater. Interfaces* **2018**, *10*, 10419.
[36] Z. Ding, C. Yuan, X. Peng, T. Wang, H. J. Qi, M. L. Dunn, *Sci. Adv.* **2017**, *3*, e1602890.
[37] W. M. Van Rees, E. A. Matsumoto, A. S. Gladman, J. A. Lewis, L. Mahadevan, *Soft Matter* **2018**, *14*, 8771.
[38] H. Huang, B. Li, J. Zhu, X. Qi, *J. Mech. Robot.* **2016**, *8*, 034503.
[39] Y. Chen, R. Peng, Z. You, *Science* **2015**, *349*, 396.
[40] W. Wang, C. Li, H. Rodrigue, F. Yuan, M.-W. Han, M. Cho, S.-H. Ahn, *Adv. Funct. Mater.* **2017**, *27*, 1604214.
[41] C. Ma, T. Li, Q. Zhao, X. Yang, J. Wu, Y. Luo, T. Xie, *Adv. Mater.* **2014**, *26*, 5665.
[42] Q. Zhao, X. Yang, C. Ma, D. Chen, H. Bai, T. Li, W. Yang, T. Xie, *Mater. Horiz.* **2016**, *3*, 422.
[43] W. Wang, N.-G. Kim, H. Rodrigue, S.-H. Ahn, *Mater. Horiz.* **2017**, *4*, 367.
[44] W. Wang, H. Rodrigue, S.-H. Ahn, *Sci. Rep.* **2016**, *6*, 20869.
[45] J. Y. Lee, W. B. Kim, W. Y. Choi, K. J. Cho, *IEEE Robot. Autom. Mag.* **2016**, *23*, 30.
[46] C. Dawson, J. Vincent, A. Rocca, *Nature* **1997**, *390*, 668.
[47] S. Sundaram, D. S. Kim, M. A. Baldo, R. C. Hayward, W. Matusik, *ACS Appl. Mater. Interfaces* **2017**, *9*, 32290.
[48] M. G. Mohammed, R. Kramer, *Adv. Mater.* **2017**, *29*, 1604965.

